





## Article

# Phytochemical, Antimicrobial, Antioxidant, and In Vitro Cytotoxicity Evaluation of *Echinops erinaceus* Kit Tan

Sherouk Hussein Sweilam <sup>1,2</sup>, Fatma M. Abdel Bar <sup>1,3</sup> , Ahmed I. Foudah <sup>1</sup> , Mohammed H. Alqarni <sup>1</sup> ,  
Nouran A. Elattal <sup>4</sup>, Omayma D. El-Gindi <sup>2</sup>, Moshera M. El-Sherei <sup>5</sup> and Essam Abdel-Sattar <sup>5,\*</sup> 

<sup>1</sup> Department of Pharmacognosy, College of Pharmacy, Prince Sattam Bin Abdulaziz University, Al-Kharj 11942, Saudi Arabia

<sup>2</sup> Department of Pharmacognosy, Faculty of Pharmacy, Egyptian Russian University, Cairo-Suez Road, Badr City, Cairo 11829, Egypt

<sup>3</sup> Department of Pharmacognosy, Faculty of Pharmacy, Mansoura University, Mansoura 35516, Egypt

<sup>4</sup> Department of Chemistry of Natural and Microbial Products, National Research Center, Dokki, Giza 12622, Egypt

<sup>5</sup> Department of Pharmacognosy, Faculty of Pharmacy, Cairo University, Kasr El-Aini Street, Cairo 11562, Egypt

\* Correspondence: [essam.abdelsattar@pharma.cu.edu.eg](mailto:essam.abdelsattar@pharma.cu.edu.eg)

**Abstract:** Wild plants are used by many cultures for the treatment of diverse ailments. However, they are formed from mixtures of many wanted and unwanted phytochemicals. Thus, there is a necessity to separate the bioactive compounds responsible for their biological activity. In this study, the chemical composition as well as antimicrobial and cytotoxic activities of *Echinops erinaceus* Kit Tan (Asteraceae) were investigated. This led to the isolation and identification of seven compounds, two of which are new (erinaceosin **C3** and erinaceol **C5**), in addition to methyl oleate (**C1**) and ethyl oleate (**C2**), loliolide (**C4**), (*E*)-*p*-coumaric acid (**C6**), and 5,7,3',5'-tetrahydroxy flavanone (**C7**). The structures of the isolated compounds were elucidated by 1D, 2D NMR, and HR-ESI-MS. The methanol extract showed the highest antimicrobial activity among the tested extracts and fractions. The *n*-hexane and EtOAc extracts showed remarkable antimicrobial activity against *B. subtilis*, *P. aeruginosa*, *E. coli*, and *C. albicans*. A cytotoxicity-guided fractionation of the most bioactive chloroform extract resulted in the isolation of bioactive compounds **C1/C2**, which showed significant cytotoxicity against HCT-116 and CACO<sub>2</sub> cell lines (IC<sub>50</sub> 24.95 and 19.74 µg/mL, respectively), followed by compounds **C3** (IC<sub>50</sub> 82.82 and 76.70 µg/mL) and **C5** (IC<sub>50</sub> 99.09 and 87.27 µg/mL), respectively. The antioxidant activity of the bioactive chloroform fractions was screened. Molecular docking was used to explain the results of the antimicrobial and anticancer activities against five protein targets, including DNA gyrase topoisomerase II, enoyl-acyl carrier protein reductase of *S. aureus* (FabI), dihydrofolate reductase (DHFR), β-catenin, and human P-glycoprotein (P-gp).

**Keywords:** *Echinops erinaceus*; antimicrobial; cytotoxicity; pseudoguaiane sesquiterpene; abscisic alcohol derivative; phenolic compounds



**Citation:** Sweilam, S.H.; Abdel Bar, F.M.; Foudah, A.I.; Alqarni, M.H.; Elattal, N.A.; El-Gindi, O.D.; El-Sherei, M.M.; Abdel-Sattar, E. Phytochemical, Antimicrobial, Antioxidant, and In Vitro Cytotoxicity Evaluation of *Echinops erinaceus* Kit Tan. *Separations* **2022**, *9*, 447. <https://doi.org/10.3390/separations9120447>

Academic Editor: Marcello Locatelli

Received: 1 December 2022

Accepted: 12 December 2022

Published: 16 December 2022

**Publisher's Note:** MDPI stays neutral with regard to jurisdictional claims in published maps and institutional affiliations.



**Copyright:** © 2022 by the authors. Licensee MDPI, Basel, Switzerland. This article is an open access article distributed under the terms and conditions of the Creative Commons Attribution (CC BY) license (<https://creativecommons.org/licenses/by/4.0/>).

## 1. Introduction

Plants of the family Asteraceae demonstrate significant therapeutic applications because of their unique and diverse pool of secondary metabolites. The reported biological activities include antioxidant, antiproliferative, anti-ulcer, and anti-inflammatory activities. They are mainly due to their wide range of phytochemicals, such as phenolics [1], sesquiterpene lactones [2], alkaloids [3,4], and triterpenes [5,6]. Traditionally, the plants of the genus *Echinops* (Asteraceae) are used to relieve gastrointestinal disturbances [7], kidney inflammation [8], microbial infections, and pain [9,10]. In addition, other reported biological properties include hepatoprotective [11], antifertility [12], analgesic, antipyretic, wound-healing, anthelmintic [13,14], and insecticidal properties [9,15]. *Echinops* spp. contains thiophenes, terpenoids (such as sesqui- and triterpenoids), phenolics (such as flavonoids,

coumarins, phenylpropanoids, and lignans), alkaloids, and essential oils [9,16]. *Echinops erinaceus* Kit Tan is an annual herbaceous plant strictly distributed in the Arabian Peninsula and is well-known in Saudi Arabia and Yemen under the name of “Alkana’a, Kanab, and Hawa elghool”. Reviewing the literature data, nothing was reported regarding the traditional uses of the plant. Our research group previously reported the phytochemical screening, antioxidant, and *in vitro* anti-inflammatory activities of *E. erinaceus* [17]. However, research studies that describe the phytochemical composition of this plant are still scarce.

Cancer is one of the most common diseases that cause death worldwide with an increased number of new cases every year. The common treatment for cancers is chemotherapy. Nowadays, patients are suffering from multidrug resistance (MDR), a phenomenon whereby cells confer drug resistance to structurally and functionally unrelated compounds. MDR may be a consequence of reduced drug influx, increased drug efflux, activation of detoxifying systems, activation of DNA repair mechanisms, evasion of drug-induced apoptosis, etc. [18]. One of the most common mechanisms in MDR is often associated with decrease in cellular drug accumulation mediated by MRP1 (ABCC1) and/or P-glycoprotein (P-gp, ABCB1). To overcome MDR, MRP1 and/or P-gp proteins inhibitors are used to block the transport function might be potentially used [19]. There is an urgent need for discovering new natural products against life-threatening multidrug-resistant microbial pathogens [20] and chemotherapy.

The current study aimed at bioguided isolation, structure elucidation, and *in vitro* biological evaluation of *E. erinaceus*. The *in vitro* biological evaluation targeted the cytotoxic activity against HCT-116 (colon carcinoma), CACO<sub>2</sub> (human colorectal intestinal carcinoma) cell lines, and its selectivity was assessed using the normal mammalian cell line, WI-38 (human lung fibroblast) using crystal violet assay. The antimicrobial activities of the fractions and the isolated compounds were performed on six pathogens, including two Gram-positive (*viz.*, *B. subtilis* and *MRSA*), two Gram-negative bacteria (*viz.*, *E. coli*, *P. aeruginosa*), a fungus (*viz.*, *A. niger*), and a yeast-like pathogen (*viz.*, *C. albicans*). Moreover, to reveal the potential molecular mechanisms responsible for the multi-biological activities of the isolated compounds, molecular docking experiments were conducted against P-glycoprotein (P-gp), a key protein in MDR of anticancer drugs [21], and human dihydrofolate reductase (DHFR) involved in malignancies and multidrug-resistance of microbial pathogens [22], in addition to DNA gyrase topoisomerase II and enoyl-acyl carrier protein reductase of *S. aureus* (FabI) as targets for bacteria and  $\beta$ -catenin as a target for cancer.

## 2. Materials and Methods

### 2.1. Plant Material and Extraction

The flowering aerial parts of *E. erinaceus* Kit Tan were collected from Riyadh region, Saudi Arabia, in March 2018 [17]. The plant material was authenticated by Mohamed Abdel-Fattah, a taxonomist and botanist, the botanical garden of the Department of Botany and Microbiology, College of Science, King Saud University. A verifier specimen (ID: 23.6.19.1-5) was placed at the local herbarium of the Pharmacognosy Department, Faculty of Pharmacy, Cairo University. The powdered shade-dried plant material was extracted and fractionated according to the method reported by Sweilam et al. (2021). The crude MeOH extract, its fractions, and the isolated compounds (C1–C7) from CHCl<sub>3</sub> fraction were subjected to *in vitro* cytotoxic and antimicrobial investigations.

### 2.2. Isolation and Purification of Compounds from the CHCl<sub>3</sub> Fraction

The powdered plant material (4 kg) was extracted by cold maceration with MeOH (5 × 10 L). The obtained extract was evaporated by a rotary evaporator (Büchi, Lugano, Switzerland) to a semisolid consistency (650 g) which was suspended in water and fractionated successively with solvents *viz.* *n*-hexane (Hex), chloroform (CHCl<sub>3</sub>), and ethyl acetate (EtOAc), to give 150 g, 50 g, and 60 g, respectively [17]. The CHCl<sub>3</sub> fraction (38 g)

was chromatographed on a Si gel column CC ( $170 \times 5 \text{ cm}^2$ ) and eluted with a mixture of  $\text{CHCl}_3/\text{MeOH}$  (100/0 to 70/30). The effluent was monitored using TLC on Si gel GF<sub>245</sub> plates and visualized by spraying with 10% vanillin- $\text{H}_2\text{SO}_4$  reagent (Flowchart S1). Fraction-1 (1.0 g) eluted with  $\text{CHCl}_3$  (100%) was further purified on a Si gel CC ( $50 \times 1 \text{ cm}^2$ ) with gradient elution (EtOAc in *n*-hexane; 1–10%) to afford subfraction-1-II (500 mg). The latter was purified on an MPLC RP-18 column (isopropanol–water, 6:4 to 10:0) to obtain compounds **C1/C2** as an unresolved mixture (methyl oleate **C1**/ethyl oleate **C2**, 9 mg). Fraction-3 (1.0 g) was subjected to a Si gel CC ( $65 \times 2 \text{ cm}^2$ ) and eluted with EtOAc in *n*-hexane (10 to 50%) to obtain subfraction-3 I-IX. Subfraction-3-II (120 mg) and subfraction-3-III (200 mg) were purified by chromatography onto an MPLC RP-18 column (MeOH- $\text{H}_2\text{O}$ , 1:1 and 3:7, respectively) to give compounds **C3** (erinaceosin, 8 mg) and **C4** (loliolide, 4.5 mg), respectively. Fraction-4 was subjected to purification on an MPLC RP-18 column (MeOH- $\text{H}_2\text{O}$ , 3:7) followed by a Sephadex LH-20 column to afford compound **C5** (erinaceol, 3 mg). In addition, Fraction-5 (1.5 g) gave subfraction-5-I (65 mg) and subfraction-5-II (36 mg) upon chromatography on a Si gel column (EtOAc in *n*-hexane; 10 to 100). Purification of subfraction-5-I and subfraction-5-II on Sephadex LH-20 columns (MeOH- $\text{CH}_2\text{Cl}_2$ , 1 to 10) resulted in the isolation of compounds **C6** (*E-p*-coumaric acid, 4 mg) and **C7** (5,7,3',5'-tetrahydroxy flavanone, 3 mg), respectively (Flowchart S1).

### 2.3. In Vitro Cytotoxicity Assay

#### 2.3.1. Materials and Cell Lines

Mammalian cell lines HCT-116 cells (human colon cancer cell line), CACO<sub>2</sub> cells (human colorectal intestinal carcinoma), and WI-38 cells (human lung fibroblast normal cells) were obtained from the American Type Culture Collection (ATCC, Rockville, MD, USA). Dimethyl sulfoxide (DMSO), crystal violet, and trypan blue dye were purchased from Sigma (St. Louis, MO, USA). Fetal Bovine serum, RPMI-1640, HEPES buffer solution, L-glutamine, gentamycin, and 0.25% Trypsin-EDTA were purchased from Lonza (Verviers, Belgium). Crystal violet stain (1%) made from 0.5% (*w/v*) crystal violet and 50% MeOH was then brought to volume with dd.H<sub>2</sub>O and filtered through a Whatmann No.1 filter paper.

#### 2.3.2. Cell Culture Condition and Propagation

The HCT-116 and CACO<sub>2</sub> cells were propagated in RPMI-1640 medium, and WI-38 cells were propagated in Dulbecco's modified Eagle's medium (DMEM), which was supplemented with 10% heat-inactivated fetal bovine serum, 1% L-glutamine, HEPES buffer, and 50 µg/mL gentamycin. All cells were maintained at 37 °C in a humidified atmosphere with 5% CO<sub>2</sub> and were subcultured two times a week [23–25].

#### 2.3.3. Cytotoxicity Evaluation Using Viability Assay

The cells were seeded in a 96-well plate at a cell concentration of  $1 \times 10^4$  cells per well in 100 µL of growth medium. Fresh medium containing different concentrations of the test sample was added after 24 h of seeding. Two-fold serial dilutions of the tested sample were added to confluent cell monolayers dispensed into 96-well, flat-bottomed microtiter plates (Falcon, NJ, USA) using a multichannel pipette. The microtiter plates were incubated at 37 °C in a humidified incubator with 5% CO<sub>2</sub> for a period of 48 h. Three wells were used for each concentration of the test sample. Control cells were incubated without a test sample and with or without DMSO. The low percentage of DMSO present in the wells (max 0.1%) was found not to affect the experiment. After incubation of the cells at 37 °C, various concentrations of samples were added, and the incubation was continued for 24 h, and viable cells' yield was determined by a colorimetric method. All experiments were carried out in triplicate [23–25].

The 50% inhibitory concentration (IC<sub>50</sub>, the concentration required to cause toxic effects in 50% of cancer cells) and the cytotoxic concentration (CC<sub>50</sub>, the concentration required to cause toxic effects in 50% of normal cells) were determined from graphic plots

of the dose–response curve for each concentration using Graphpad Prism software (San Diego, CA, USA).

#### 2.4. In Vitro Antimicrobial Activity

The antimicrobial activity of *E. erinaceus* extracts was tested by the agar well diffusion method [26] against six micro-organisms (*Bacillus subtilis*, MRSA, *Pseudomonas aeruginosa*, and *Escherichia coli* on nutrient agar, and *Candida albicans*, and *Asperigillus niger* on potato dextrose agar, PDA). In this experiment, all extracts were dissolved in MeOH (200 µg/mL), and 50 µL of the prepared sample solution was added to each well, separately in each case. The diameter of inhibition zone (DIZ) was measured.

#### 2.5. In Vitro Antioxidant Effect

The *in vitro* antioxidant activity of fractions 3, 4, and fraction 5 of the CHCl<sub>3</sub> extract (Flowchart S1) was established in accordance with Burits and Bucar [27]. In brief, 50 µL of the sample solution (200 µg/mL) was added to 100 µL of 2,2-diphenyl-1-picrylhydrazyl (DPPH) methanolic solution (0.1%). After a period of 50 min incubation in the dark, absorbance was measured at 517 nm against the blank. The inhibition percentage of DPPH free radicals (I) was as follows:

$$I (\%) = (A \text{ blank} - B \text{ sample} / A \text{ blank}) \times 100$$

where A (blank) is the absorbance of control (containing all reagents, except the test compound), and B (sample) is the absorbance of the test sample; ascorbic acid is used as a standard drug.

#### 2.6. In Silico Studies of the Isolated Compounds

##### 2.6.1. PASS and ADME Predictions

The isolated compounds (Figure 1), namely, methyl oleate (C1), ethyl oleate (C2), erinaceosin (C3), loliolide (C4), erinaceol (C5), (*E*)-*p*-coumaric acid (C6), and 5,7,3',5'-tetrahydroxy flavanone (C7), were drawn by MarvinSketch program and simulated by the Prediction of Activity Spectra for Substances (PASS) and Absorption, Distribution, Metabolism, and Elimination (ADME) prediction web tools. The isolated compounds were analyzed by SwissADME online free site for prediction of physicochemical properties, drug likeness, solubility, and pharmacokinetics [28–30].

##### 2.6.2. Molecular Docking Analysis

Docking analyses of the isolated compounds were accomplished to understand the antibacterial and anticancer activities. For antibacterial activity, DNA gyrase topoisomerase II (*E. coli*) enzyme (PDB ID: 1KZN) [31] and enoyl-acyl carrier protein reductase of *S. aureus*, FabI (PDB ID: 3GNS) [32] were used as the target proteins. For anticancer activity, β-catenin in complex with compound 6 (PDB ID: 7AFW) [33] was used. For both activities, dihydrofolate reductase (DHFR) (PDB ID: 4M6J) [34] has been chosen as the target protein. The study of the MDR of the anticancer and antimicrobial candidates, the human P-gp (PDB ID: 6C0V) [21], were downloaded from PDB (<https://www.rcsb.org> (accessed on 1 December 2022)). The downloaded proteins were prepared by removing water and any unwanted residual matter and adding non-hydrogen atoms by PyMOL 2.3. The PyRx Autodock Vina (Scripps Research, La Jolla, CA, USA) was utilized for these *in silico* studies. The co-crystallized ligands, including clorobiocin, triclosan, 3-[(24-methyl-5-oxidanylidene-2,3-dihydro-1,4-benzoxazepin-2-yl)]benzenecarbonitrile (R9Q), ciprofloxacin, and methotrexate for studying the comparative binding affinity to the target proteins, were downloaded and saved in 3D SDF format.

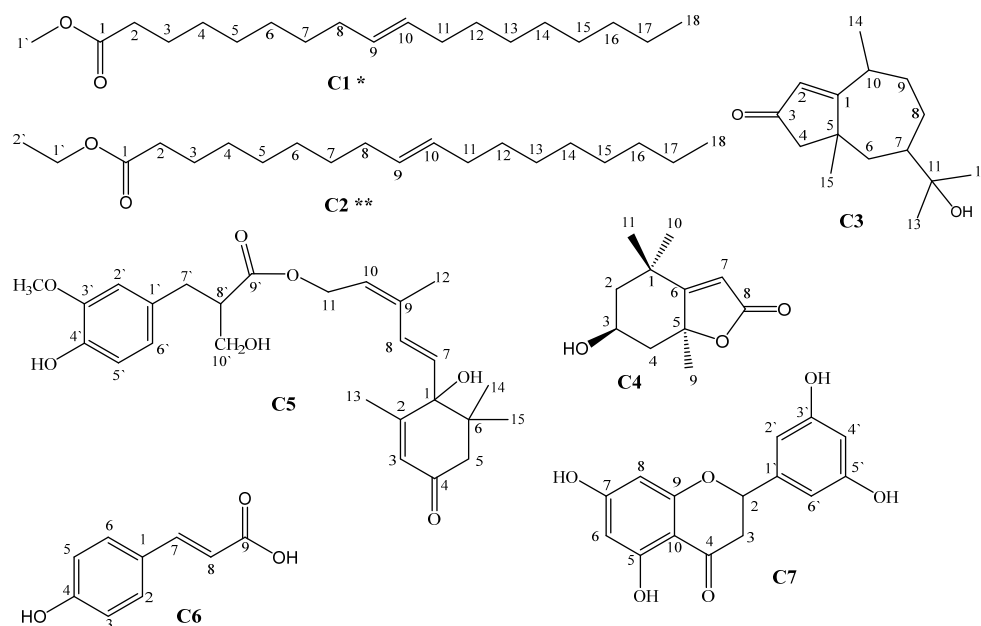


**Figure 1.** Structures of isolated compounds from *Echinops erinaceus* (C1, C2, C3–C7).

### 3. Results and Discussion

#### 3.1. Identification of the Isolated Compounds

The spectral data of the known compounds (C1, C2, C4, C6, and C7) are recorded in Tables S1–S4, while the spectra of all isolated compounds (C1–C7) are displayed in Figures S1–S37.

##### 3.1.1. Identification of Compounds C1 and C2

The mixture of compounds C1 and C2 was identified as a mixture of two esterified mono-unsaturated long-chain fatty acids using 1D, 2D NMR, and ESI-MS data (Figure 1, Table S1) [35,36]. It is worth noting that methyl oleate (C1) has been isolated before from the *Echinops* genus [37]; however, this is the first report on the identification of ethyl oleate (C2) from the *Echinops* genus, although it was reported before in the Asteraceae family [38].

##### 3.1.2. Identification of Compound C3

According to HR-ESI-MS, compound C3 had a molecular formula of  $C_{15}H_{24}O_2$  based on the ion peak at  $m/z$  237.1859 [ $M + H$ , 1.5%] (calcd. 237.1855) and 219.1753 [ $M^+ - OH$ , 85%] (calcd. 219.1749). The NMR spectral data of compound C3 (Table 1) were consistent with the basic skeleton of pseudoguaiane sesquiterpenes, except for the presence of the  $\alpha$ ,  $\beta$ -unsaturated ketone of a cyclopentenone ring observed at positions 1, 2, and 3 [39]. The  $^1H$ -NMR spectrum of C3 exhibited four methyl signals at  $\delta_H$  1.09 (s, C-13), 1.07 (s, C-12), 1.04 (s, C-15), and 0.96 (d,  $J = 6.7$  Hz, C-14), which were correlated in the HSQC spectrum with the carbon signals at  $\delta_C$  28.1, 26.1, 20.1, and 16.2, respectively. The  $^{13}C$ -NMR spectrum displayed fifteen carbon signals, categorized as four methyls ( $\delta_C$  26.1, 28.1, 20.1, and 16.2 assigned to C-12, C-13, C-15, and C-14, respectively), four methylenes ( $\delta_C$  43.5, 35.9, 30.6, and 27.6 assigned to C-4, C-6, C-9, and C-8, respectively), three methines ( $\delta_C$  125.9, 43.4, and 36.5 assigned to C-2, C-7, and C-10, respectively), and four quaternary carbon atoms at  $\delta_C$  202.5 (C-3), 179.8 (C-1), 73.4 (C-11), and 41.9 (C-5). These data, along with additional information provided by  $^1H$ - $^1H$  spin interactions between the coupled protons for H-6/H-7, H-7/H-8, H-8/H-9, and H-9/H-10, were observed in the COSY spectrum (Table 1 and Figure S11) establishing a heptocyclic moiety of the sesquiterpene skeleton. The HMBC correlations (Figures 2 and S12) between the protons at  $\delta_H$  1.07 (s, H-12) and 1.09 (s, H-13) with the carbon signals at  $\delta_C$  73.4 (C-11) and 43.4 (C-7) indicated the presence of a

hydroxyisopropyl group attached to C-7. In addition, the presence of HMBC correlations of H-2/C-5 and H-2/C-9 and H-4/C-1, H-4/C-2, H-4/C-3, H-4/C-5, and H-4/C-6 confirmed the presence of a cyclopentanone ring system. From the aforementioned data, compound **C3** was identified as a new natural compound named erinaceosin (Figure 1).

**Table 1.** NMR spectral data of compound **C3** in CD<sub>3</sub>OD (500 MHz for <sup>1</sup>H- and 125 MHz for <sup>13</sup>C-NMR).

	HSQC			HMBC (H→C)			COSY
	Type	$\delta_H$ (J in Hz)	$\delta_C$	$^2J_{CH}$	$^3J_{CH}$	$^4J_{CH}$	$^1H$ - $^1H$
1	C		179.8				
2	CH	5.76, <i>s</i>	125.9		C-5	C-9	
3	C=O		202.5				
4	CH <sub>2</sub>	2.27, <i>m</i> ; 2.21, <i>m</i> , overlapped	43.5	C-3, C-5	C-1, C-2, C-6		
5	C		41.9				
6	CH <sub>2</sub>	1.23, <i>m</i> ; 1.88, <i>m</i>	35.9	C-5	C-1, C-8, C-11	C-10, C-13	H-7
7	CH	1.36, <i>m</i>	43.4	C-6, C-11	C-9	C-4	H-6, H-8
8	CH <sub>2</sub>	1.67, <i>m</i>	27.6	C-9	C-11	C-1	H-7, H-9
9	CH <sub>2</sub>	2.21, <i>m</i> , overlapped; 2.50, <i>m</i>	30.6		C-1,	C-2, C-5, C-6	H-10, H-8
10	CH	2.22, overlapped	36.6	C-1	C-2, C-5	C-3, C-7	H-14
11	C		73.4				
12	CH <sub>3</sub>	1.07, <i>s</i>	26.1	C-11		C-6, C-8	
13	CH <sub>3</sub>	1.09, <i>s</i>	28.1	C-11	C-12		
14	CH <sub>3</sub>	0.96, <i>d</i> (6.7)	16.2	C-10		C-5	H-10
15	CH <sub>3</sub>	1.04, <i>s</i>	20.1	C-5	C-1, C-4, C-6		

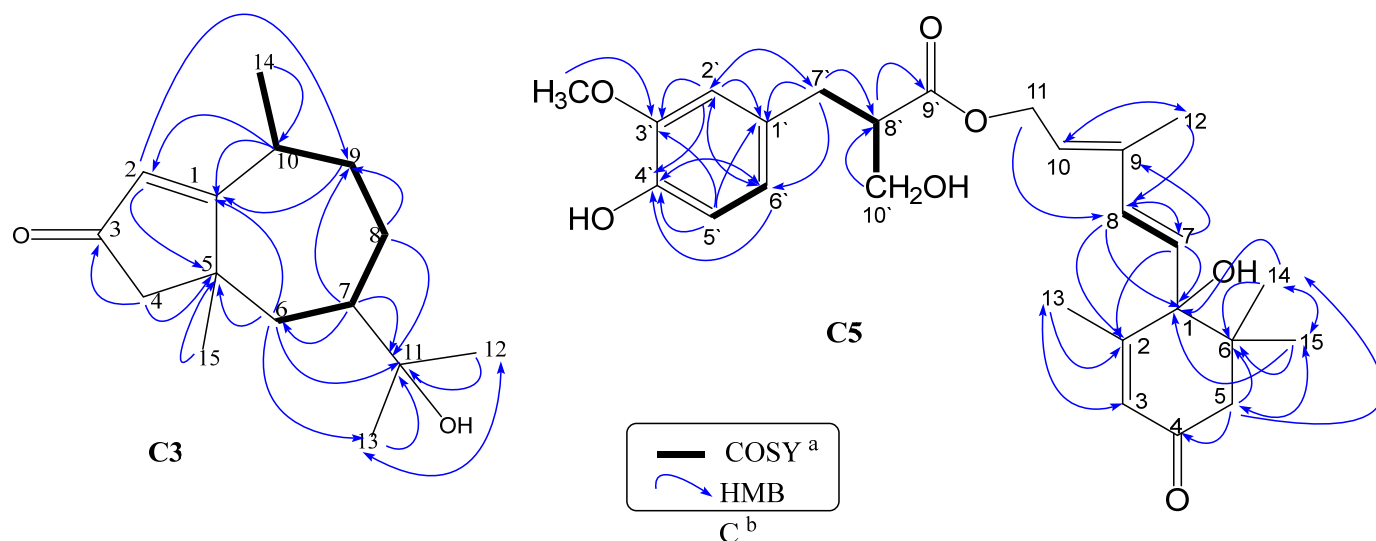


**Figure 2.** (a) Selected COSY correlations and (b) HMBC correlations of the new compounds (**C3** and **C5**).

### 3.1.3. Identification of Compound **C4**

The HR-ESI-MS of compound **C4** (Figure S21) indicated a molecular formula of C<sub>11</sub>H<sub>16</sub>O<sub>3</sub> based on the ion peak at *m/z* 197.1156 [M + H]<sup>+</sup>, 100%; 219.0973 [M + Na]<sup>+</sup>, 70%. The detailed study of MS, 1D, and 2D NMR data (Table S2 and Figures S14–S20) identified the structure of **C4** as lolilide, which was further confirmed by comparison

of its spectral data with those reported in the literature. This compound was reported from genus *Echinops* for the first time and previously isolated from *Codium tomentosum* and *Xanthium spinosum* [40,41].

### 3.1.4. Identification of Compound C5

Compound C5 displayed an  $m/z$  of 575.1975  $[M + 3K]^+$  (100%, cal. 575.1216) in the positive mode of the HR-ESI-MS spectrum (Figure S29) coincident with a molecular formula of  $C_{26}H_{34}O_7K_3$ . One- and two-dimensional NMR spectral data of C5 (Table 2 and Figures S22–S27) showed the possible presence of an abscisic alcohol moiety [42–45], which was confirmed by the presence of four tertiary methyl singlets at  $\delta_H$  1.85 (H<sub>3</sub>-12;  $\delta_C$  20.2), 1.95 (H<sub>3</sub>-13;  $\delta_C$  21.8), 0.98 (H<sub>3</sub>-14;  $\delta_C$  24.1), and 0.94 (H<sub>3</sub>-15;  $\delta_C$  25.2); two *trans*-coupled olefinic proton doublets at  $\delta_H$  7.66 ( $J = 16.1$  Hz, H-8;  $\delta_C$  129.9) and 6.13 ( $J = 16.1$  Hz, H-7;  $\delta_C$  138.2); and two proton signals at  $\delta_H$  5.67 (1H, *br.s*, H-10;  $\delta_C$  120.4) and 5.85 (1H, *s*, H-3;  $\delta_C$  128.0). The latter two double bonds,  $^{2(3)}$  and  $^{9(10)}$ , bear two methyl substituents (i.e., H<sub>3</sub>-13 and H<sub>3</sub>-12) attached to C-2 ( $\delta_C$  152.2) and C-9 ( $\delta_C$  131.0), respectively. The presence of a hydroxy methylene group was assigned based on the proton multiplet at  $\delta_H$  3.45 (H-11;  $\delta_C$  62.6). The triene system ( $\Delta^{2(3)}$ ,  $\Delta^{7(8)}$ , and  $\Delta^{9(10)}$ ) is connected to a carbonyl carbon at  $\delta_C$  203.0 (C-4), and the connection was confirmed by the HMBC spectrum. This was evident from the HMBC correlations of the two methylene proton signals at  $\delta_H$  2.11 and 2.45 (H<sub>a</sub>-5 and H<sub>b</sub>-5) with the ketonic group at C-4. Other significant HMBC correlations, including H<sub>a</sub>-5/C-1, H-14/C-1, H-15/C-1, H-13/C-2, H-12/C-8, H-3/C-13, H-3/C-1, H-7/C-1, H-8/C-1, and H-11/C-8, were also used to confirm the presence of an abscisic alcohol moiety (Table 2 and Figure S27).

In addition to the abscisic alcohol moiety, a set of aromatic ABX systems were revealed from the doublet signal at  $\delta_H$  6.70 (*d*,  $J = 7.8$  Hz, H-5'), a broad doublet at  $\delta_H$  6.45 (*br.d*,  $J = 7.8$  Hz, H-6'), and a broad singlet at  $\delta_H$  6.49 (1H, *br.s*, H-2'), which are directly correlated to carbon signals at  $\delta_C$  116.2, 123.2, and 113.7, respectively (HSQC). The singlet proton signal at  $\delta_H$  3.64 (3H, *s*) correlated with the carbon at  $\delta_C$  56.6 (HSQC) and was assigned to a *m*-methoxy substituent at C-3' of the aromatic ring. A third moiety formed from a 3-hydroxy-2-methylpropanoic acid chain (HMPA) was attached to C-1' of the aromatic ring and esterified the abscisic alcohol moiety at C-11. The HMPA moiety was deduced from the presence of a terminal hydroxy methylene group revealed from a proton signal that appeared as a doublet of doublet ( $J = 8.8, 4.5$  Hz; H-10') overlapped with the proton multiplet of H<sub>2</sub>-11 of the abscisic alcohol moiety at  $\delta_H$  3.45 (4H). This proton signal is directly correlated with the carbon at  $\delta_C$  62.6 (i.e., coincident signals of C-10'/C-11). Additionally, the NMR data revealed the presence of two proton multiplets of a methylene group of H<sub>2</sub>-7' ( $\delta_H$  2.49 and 2.65;  $\delta_C$  36.5), which is correlated in the HMBC spectrum with C-8, C-1', C-2', and C-6', confirming its attachment to the aromatic ring. Finally, the proton signal at  $\delta_H$  1.84 (1H, *m*, H-8',  $\delta_C$  44.5), forming the branching point of the side chain formed by C7'-C-8'-C-10', showed an HMBC correlation with the ester carbonyl group at  $\delta_C$  169.4 (C-9'). The above-mentioned data suggested a 4-(3-hydroxypropyl)-2-methoxyphenol moiety that is closely related to the previously published data of 5-(3-hydroxypropyl)-2-methoxyphenol derivative [46]. The analysis of the COSY and HMBC spectra of compound C5 (Table 2) established the connections of the assigned protons and carbons. From the aforementioned discussion, the structure of C5 was confirmed to be a new derivative composed of an abscisic alcohol moiety esterified with a modified phenylpropane carboxylic acid moiety and was named erinaceol, which is recorded herein for the first time from nature.

### 3.1.5. Identification of Compound C6

Compound C6 was identified as (*E*)-*p*-coumaric acid from the  $^1H$ -NMR and APT spectra (Table S3 and Figures S30 and S31) and by co-chromatography with an authentic sample of (*E*)-*p*-coumaric acid, which was isolated for the first time from *E. erinaceus* [47].

### 3.1.6. Identification of Compound C7

The spectral analysis of C7 (Table S4 and Figures S32–S37) confirmed its structure as 5,7,3',5'-tetrahydroxy flavanone [48], and it is worth mentioning that this is the first report of C7 from *Echinops* spp.

**Table 2.** NMR spectral data of compound C5 in CD<sub>3</sub>OD (500 MHz for <sup>1</sup>H- and 125 MHz for <sup>13</sup>C-NMR).

C/H#	HSQC			HMBC (H→C)			COSY
	Type	δ <sub>H</sub> (J in Hz)	δ <sub>C</sub>	<sup>2</sup> J <sub>CH</sub>	<sup>3</sup> J <sub>CH</sub>	<sup>4</sup> J <sub>CH</sub>	<sup>1</sup> H- <sup>1</sup> H
<b>Abscisic alcohol moiety</b>							
1	C		82.1				
2	C		152.2				
3	CH	5.85, 1H, <i>s</i>	128.0		C-1, C-13		
4	C		203.0				
5	CH <sub>2</sub>	2.11, <i>m</i> ; 2.45, <i>m</i>	51.1	C-4, C-6	C-1, C-14, C-15		
6	C		43.4				
7	CH	6.13, <i>d</i> (16.1)	138.2	C-1, C-8	C-2, C-9		H-7
8	CH	7.66, <i>d</i> (16.1)	129.9	C-7	C-1, C-10, C-12	C-2	H-8
9	C		131.0				
10	CH	5.67, <i>br.s</i>	120.4	C-9	C-12		
11	CH <sub>2</sub>	3.45, <i>m</i> <sup>a</sup>	62.6 <sup>b</sup>	C-8	C-8'		
12	CH <sub>3</sub>	1.85, <i>s</i>	20.2		C-8, C-10	C-9'	
13	CH <sub>3</sub>	1.95, <i>s</i>	21.7	C-2	C-1, C-3		
14	CH <sub>3</sub>	0.98, <i>s</i>	24.1	C-6	C-1, C-5, C-15		
15	CH <sub>3</sub>	0.94, <i>s</i>	25.1	C-6	C-1, C-5, C-14	C-4	
<b>4-(3-Hydroxypropyl)-2-methoxyphenol moiety</b>							
1'	C		134.4				
2'	CH	6.49, <i>br. s</i>	113.7	C-3'	C-4', C-7', C-6'		
3'	C		149.3				
4'	C		146.4				
5'	CH	6.70, <i>d</i> (7.8)	116.2	C-4'	C-3', C-1'		H-6'
6'	CH	6.45, <i>br. d</i> (7.9)	123.2		C-4', C-2'		H-5'
7'	CH <sub>2</sub>	2.49, <i>m</i> ; 2.65, <i>m</i>	36.5	C-1', C-8'	C-2', C-6'		H-8'
8'	CH	1.84, <i>m</i>	44.5	C-9'			H-7', H-10'
9'	C		169.4				
10'	CH <sub>2</sub>	3.45, <i>dd</i> (8.8, 4.5) <sup>a</sup>	62.6 <sup>b</sup>	C-8'			
	O-CH <sub>3</sub>	3.64, <i>s</i>	56.6		C-3'		

<sup>a, b</sup> Similar letters indicate coincident signals.

### 3.2. Biological Activities of Main Fractions and Isolates from *E. erinaceus*

#### 3.2.1. In Vitro Cytotoxic Activity

The results of bio-guided cytotoxic activity against HCT-116 and CACO<sub>2</sub> cells of the different extracts showed that the CHCl<sub>3</sub> extract showed the highest activity among the



tested extracts (Table 3). However, it exhibited moderate cytotoxic activity with IC<sub>50</sub> of 67.30 ± 4.87 and 81.95 ± 4.63 µg/mL with a selectivity index (SI) > 1 (1.73 and 1.42) against HCT-116 and CACO<sub>2</sub> cells, respectively. Further bio-guided fractionation of the CHCl<sub>3</sub> extract revealed that fractions Fr.1, Fr.3, and Fr.4 were the most active among the tested fractions. Considering Fr.1, it showed the strongest activity with IC<sub>50</sub> of 14.93 ± 1.28 and 10.50 ± 0.61 µg/mL and SI of 3.37 and 4.80 against HCT-116 and CACO<sub>2</sub> cells, respectively. Compound C1/C2 showed significant antiproliferative activity with IC<sub>50</sub> of 24.95 ± 1.23 and 19.74 ± 1.94 µg/mL and good SI (1.95 and 2.47) against the tested cells, respectively. The new compound (C3) purified from Fr.3 showed a weak cytotoxic activity (IC<sub>50</sub> 82.82 ± 3.94 and 99.09 ± 5.84 µg/mL) with good SI (2.15 and 1.80), respectively. Similarly, compound C5 obtained from Fr.4 showed weak cytotoxicity (IC<sub>50</sub> 76.70 ± 3.71 and 87.27 ± 4.67 µg/mL, respectively) and good SI (2.12 and 1.87, respectively) (Table 3).

**Table 3.** *In vitro* cytotoxic activity (IC<sub>50</sub>, µg/mL), selectivity index (SI) of the different extracts, fractions, and compounds C1–C7 from *E. erinaceus*.

Test Sample	IC <sub>50</sub> (µg/mL)		CC <sub>50</sub> (µg/mL)	Selectivity Index (SI)	
	HCT-116 <sup>a</sup>	CACO <sub>2</sub> <sup>a</sup>	WI-38 <sup>a</sup>	HCT-116	CACO <sub>2</sub>
<b>Extract</b>					
Total MeOH	165.92 ± 9.82	192.82 ± 12.86	226.14 ± 11.82	1.36	1.17
<i>n</i> -Hex	88.91 ± 5.42	87.93 ± 4.89	110.79 ± 7.43	1.25	1.26
CHCl <sub>3</sub>	67.30 ± 4.87 <sup>''</sup>	81.95 ± 4.63 <sup>''</sup>	116.53 ± 9.27	1.73	1.42
EtOAc	170.84 ± 10.29	218.72 ± 11.04	246.41 ± 14.23	1.44	1.13
Re. Aq	323.25 ± 15.83	361.08 ± 18.24	449.72 ± 21.34	1.39	1.25
<b>* CHCl<sub>3</sub> Fractions</b>					
* Fr.1	14.93 ± 1.28 <sup>''</sup>	10.50 ± 0.61 <sup>''</sup>	50.36 ± 3.80	3.37	4.80
* Fr.3	30.94 ± 1.78 <sup>''</sup>	38.9 ± 1.89 <sup>''</sup>	60.62 ± 3.42	1.96	1.56
* Fr.4	24.93 ± 1.29 <sup>''</sup>	12.95 ± 0.61 <sup>''</sup>	53.24 ± 3.08	2.14	4.11
* Fr.5	83.41 ± 4.03	101.78 ± 4.08	117.64 ± 6.72	1.41	1.16
* Fr.6	54.43 ± 2.19	59.85 ± 2.73	105.31 ± 4.93	1.93	1.76
<b>Compounds</b>					
C1/C2	24.95 ± 1.23 <sup>''</sup>	19.74 ± 1.94 <sup>''</sup>	48.75 ± 3.91	1.95	2.47
C3	82.82 ± 3.94 <sup>''</sup>	99.09 ± 5.84 <sup>''</sup>	178.02 ± 8.74	2.15	1.80
C4	173.12 ± 9.74	217.25 ± 8.73	272.93 ± 16.25	1.58	1.26
C5	76.70 ± 3.71 <sup>''</sup>	87.27 ± 4.67 <sup>''</sup>	162.84 ± 7.08	2.12	1.87
C6	179.81 ± 14.08	425.48 ± 16.71	416.52 ± 18.96	2.32	0.98
C7	219.35 ± 9.76	284.73 ± 14.93	382.53 ± 17.21	1.74	1.34
Vin <sup>b</sup>	2.35 ± 0.41	2.62 ± 0.44	13.98 ± 1.34	5.95	5.34

<sup>a</sup> Samples were analyzed in triplicate (*n* = 3) and expressed as mean ± standard deviation; <sup>b</sup> Vin: Vinblastine Sulfate (Reference standard drug); MeOH = methanol extract; *n*-Hex = *n*-hexane extract; CHCl<sub>3</sub> = chloroform extract; EtOAc = ethyl acetate extract; Re.Aq = remaining aqueous extract; \* Chloroform fractions; HCT-116 = human colon cancer cell line; CACO<sub>2</sub> = human colorectal intestinal carcinoma cells; WI-38 = human lung fibroblast normal cells. <sup>''</sup> IC<sub>50</sub> (µg/mL): 1–10 = very strong, 11–20 = strong, 21–50 = moderate, 51–100 = weak, and above 100 = non-cytotoxic [49].

### 3.2.2. *In Vitro* Antimicrobial Activity

The different extracts and fractions of *E. erinaceus* were tested for their antimicrobial activity against a panel of pathogenic micro-organisms, including two strains of Gram-positive bacteria (*Bacillus subtilis* and methicillin-resistant *Staphylococcus aureus*, MRSA), two strains of Gram-negative bacteria (*Pseudomonas aeruginosa* and *Escherichia coli*), and two

fungus and yeast-like micro-organisms (*Asperigillus niger* and *Candida albicans*), using the agar well diffusion assay by measuring the diameter of inhibition zone (DIZ). The results of the antibacterial properties of the plant extracts (Table 4) demonstrated that the total MeOH extract had the highest antimicrobial activity against all the tested strains, except against MRSA. It showed significant antibacterial activity against *B. subtilus* ( $27.5 \pm 0.7$  mm), which is more active than the reference drug, streptomycin ( $18 \pm 1.41$  mm). It also showed a pronounced antifungal activity against *C. albicans* ( $26 \pm 1.41$  mm), which is almost comparable to the reference drug, clotrimazole ( $28 \pm 2.82$  mm). This was followed by the *n*-hexane and EtOAc extracts, which showed strong antibacterial and antifungal activities. However, no antimicrobial activity against MRSA was detected in any of the investigated *E. erinaceus* samples. The CHCl<sub>3</sub> extract showed good activity against *B. subtilis* ( $20.5 \pm 1.41$  mm), *P. aeruginosa* ( $17.5 \pm 1.41$  mm), and *E. coli* ( $18 \pm 1.41$  mm) test strains. Fr.3 of the CHCl<sub>3</sub> extract showed the highest antimicrobial effect compared to other fractions against the same bacterial strains as its main extract. However, the CHCl<sub>3</sub> extract and its fractions (Fr.3, Fr.4, and Fr.5) showed no activity against the tested fungal strains, *C. albicans* and *A. niger*. The aqueous extract showed good activity against all strains, except MRSA and *A. niger* (Table 4).

**Table 4.** Antimicrobial activity of the extracts and selected fractions of *E. erinaceus* against a selected group of bacterial and fungal pathogens.

Bacterial Isolates	Gram-Positive		Gram-Negative		Fungi and Yeast	
	<i>B. subtilus</i> (a)	MRSA(a)	<i>P. aeruginosa</i> (a)	<i>E. coli</i> (a)	<i>C. albicans</i> (b)	<i>A. niger</i> (b)
	ATCC6633	ATCC25923	ATCC27953	ATCC25922	NRRLY477	NRRL599
MeOH ext.	27.5 ± 0.7	-	23.5 ± 0.7	24 ± 1.41	26 ± 1.41	16 ± 1.41
<i>n</i> -hex ext.	22.5 ± 0.7	-	22 ± 2.82	22.25 ± 1.76	22.5 ± 2.82	-
CHCl <sub>3</sub> ext.	20.5 ± 1.41	-	17.5 ± 1.41	18 ± 1.41	-	-
EtOAc ext.	20.0 ± 1.41	-	22 ± 1.41	21.5 ± 0.7	22 ± 1.41	12.5 ± 0.7
Re. Aq. ext.	18.5 ± 2.12	-	17 ± 1.41	20.5 ± 2.12	18 ± 1.41	-
* Fr.3	17.5 ± 0.7	-	16 ± 1.41	17.25 ± 2.82	-	-
* Fr.4 *	14.5 ± 2.12	-	14 ± 0.71	16 ± 0.7	-	-
* Fr.5 *	17 ± 1.41	-	14 ± 1.41	14.5 ± 0.7	-	-
Streptomycin <sup>a</sup>	18 ± 1.41	20 ± 1.41	27 ± 1.41	25 ± 2.82	-	-
Clotrimazole <sup>b</sup>	-	-	-	-	28 ± 2.82	26 ± 1.41

Antimicrobial activity of bacterial isolates by agar diffusion method. (a) Grown on nutrient medium agar; (b) on potato dextrose agar (PDA); diameter of inhibition zone (IZD) measured in mm. Each value is expressed as mean ± SD, pore size 5 mm; -: negative; MeOH = methanol extract; *n*-hex = *n*-hexane extract; CHCl<sub>3</sub> = chloroform extract; EtOAc = ethyl acetate extract; and Re. Aq = remaining aqueous extract, tested at a concentration of 200 µg/mL (50 µL/well); \* CHCl<sub>3</sub> fractions. <sup>a</sup>: Streptomycin (10 µg/mL) and <sup>b</sup>: Clotrimazole (15 µg/mL).

### 3.2.3. Antioxidant Activity

DPPH free radical scavenging activities of Fr.3, Fr.4, and Fr.5 of the CHCl<sub>3</sub> fraction were assessed. Fr.3 exhibited remarkable free radical scavenging activity (55%), whereas the lowest activity was observed for sample Fr.4 (32%) (Figure 3).

### 3.3. PASS and ADME Predictions of the Isolated Compounds

The isolated compounds were sketched using the MarvinSketch program and simulated by the Prediction of Activity Spectra for Substances (PASS) and Absorption, Distribution, Metabolism, and Elimination (ADME) prediction web tools [28–30]. The PASS tool predicted several biological activities. The isolated compounds (C1/C2, C3–C7) displayed significant probable activity “Pa” ranges, including antioxidant (0.828–0.297), anticancer (0.746–0.343), anti-inflammatory (0.717–0.325), antifungal (0.593–0.364), and antibacterial

(0.455–0.176) activities (Table S5). The ADME prediction results showed that all compounds showed a great bioavailability score ranging from 0.85 to 0.55 and fulfilled all drug-likeness rules and synthetic accessibility (1.61–4.14), which showed an explicit synthetic route. Additionally, all compounds were predicted to be moderate to very soluble in water. In addition, skin permeation and ADME properties were analyzed by the Swiss-ADME software, as recorded in Table S5. The BOILED-Egg method [50] showed that compounds C3–C6 have high GI absorption properties with high predicted diffusion through the BBB and good skin permeability (log Kp). However, compound C7 showed high predictable GI absorption and skin permeability properties but may diffuse poorly through the BBB [51]. Compounds C1–C6 showed no predictable binding to P-gp, except for C7, which may suffer from cellular efflux. Regarding inhibition of metabolic enzymes, compound C1 may inhibit CYP1A2, whereas C7 may inhibit CYP3A4, resulting in potential drug–drug interactions and adverse effects [28]. The findings revealed that five out of the seven compounds fulfilled the oral drug ability of Lipinski’s rule of five (RO5), while two slightly met the criteria of RO5.

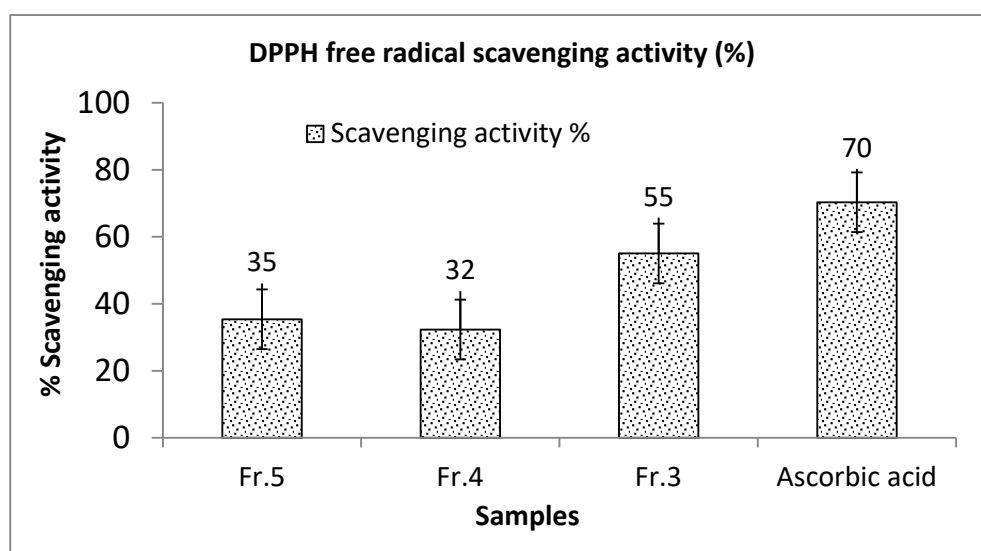


**Figure 3.** DPPH free radical scavenging activity (%). The results are the average of two replicate experiments, and the error bars show standard deviations.

### 3.4. *In Silico* Docking Study of the Isolated Compounds

A docking study was executed for the isolated compounds from *E. erinaceus* against five explored molecular targets, including DNA gyrase topoisomerase II (PDB ID: 1KZN) [31], enoyl-acyl carrier protein reductase of *S. aureus*, FabI (PDB ID: 3GNS) [32], and dihydrofolate reductase (DHFR) (PDB ID: 4M6J) [34] as targets for bacteria, and  $\beta$ -catenin (PDB ID: 7AFW) [33] in addition to human P-glycoprotein (P-gp) (PDB ID: 6C0V) [21] as targets for cancer. The results showed that the isolated phenolics and sesquiterpenes were predicted to have remarkable *in silico* binding affinities against the investigated molecular targets.

#### 3.4.1. Docking against Antimicrobial Molecular Targets Interactions with DNA Gyrase Topoisomerase II

DNA gyrase topoisomerase II is a bacterial enzyme that regulates the topological properties of bacterial DNA, especially of *E. coli*. Compounds (C1–C6) demonstrated moderate–weak binding affinities toward this protein, as depicted by their binding free energy (BFE) values ranging from  $-4.1$  to  $-5.7$  kcal/mol (Table S6) compared to the reference ligand, clorobiocin (CBN,  $-7.4$  kcal/mol). Of these, compound C3 (BFE,  $-5.7$  kcal/mol) showed H-bonding interactions with Ala96 and the crucial amino acid, Gly117 (Figure 4a), while compound C5 (BFE,  $-5.7$  kcal/mol) showed H-bonding interactions with Ala96 and Ser121

(Figure 4b) [52]. On the other hand, compound C7 exhibited better BFE ( $-7.7$  kcal/mol) than CBN, which can be explained by the presence of several binding interactions with the amino acid residues (Table S6), including strong H-bondings with Glu42, Ser121, and the crucial Val120 residue (Figure 4c) [52]. Therefore, C7 could contribute to the antibacterial activity of MeOH and  $\text{CHCl}_3$  extracts.

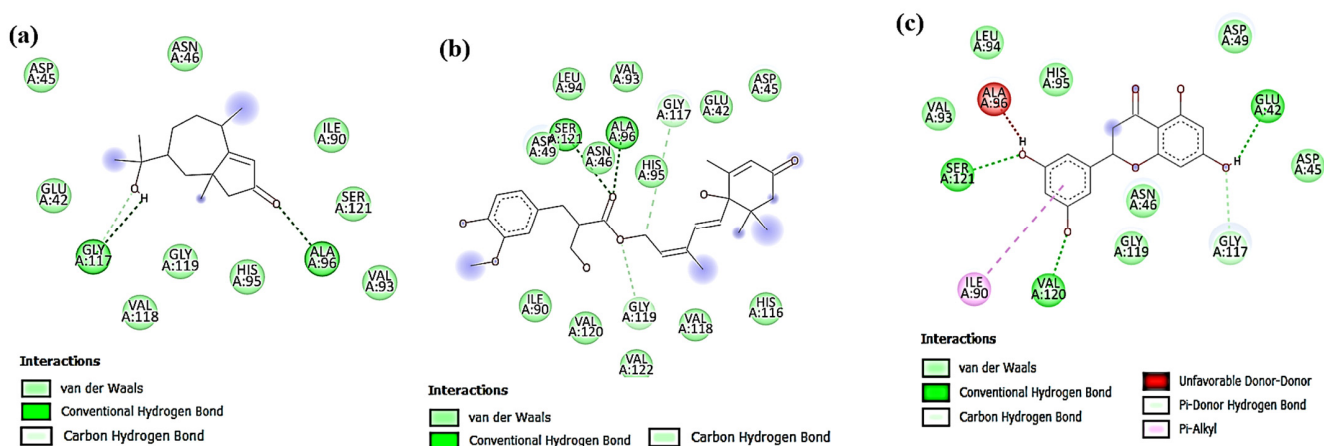


**Figure 4.** Two-dimensional (2D) molecular interactions of (a) Compound C3; (b) Compound C5; and (c) Compound C7 with the active site of DNA gyrase topoisomerase II (*E. coli*) enzyme (PDB ID:1KZN), (dimensions X:21.0176, Y: 30.3575, Z:27.6357), (root mean square deviation) RMSD < 2.

#### Interactions with Enoyl-Acyl Carrier Protein Reductase (FabI)

FabI protein is one of the critical targets for discovering antimicrobial compounds. It has been found in several bacteria, especially in *E. coli* and *S. aureus*. From the docking results (Table S6), compounds C4, C-5, and C6 have comparable BFE values ( $-5.9$ ,  $-6.0$ , and  $-5.8$  kcal/mol, respectively) to the reference FabI inhibitor, Triclosan (BFE,  $-5.8$  kcal/mol) [32], while C3 and C7 have greater BFE ( $-6.3$  and  $-6.9$  kcal/mol, respectively). It was observed that the new compound C3 showed strong H-bonding interactions with Tyr39, Arg45, Gln64, and Glu72 (Figure 5a), whereas compound C5 (Figure 5b) shared Triclosan in binding with the amino acids Ile20 and Leu196 through the  $\pi$ -alkyl/alkyl interaction and formed strong H-bondings with Gly13, Ala21, Ser93, and Ser121 [52]. Finally, C7 was able to interact with several residues, such as Ala15, Ile20, Gly13, and Ser93 (Table S6 and Figure 5c). Consequently, it could be concluded that compounds C3–C5 and C7 may be participating in the observed antimicrobial activities of the investigated *E. erinaceus* extracts.

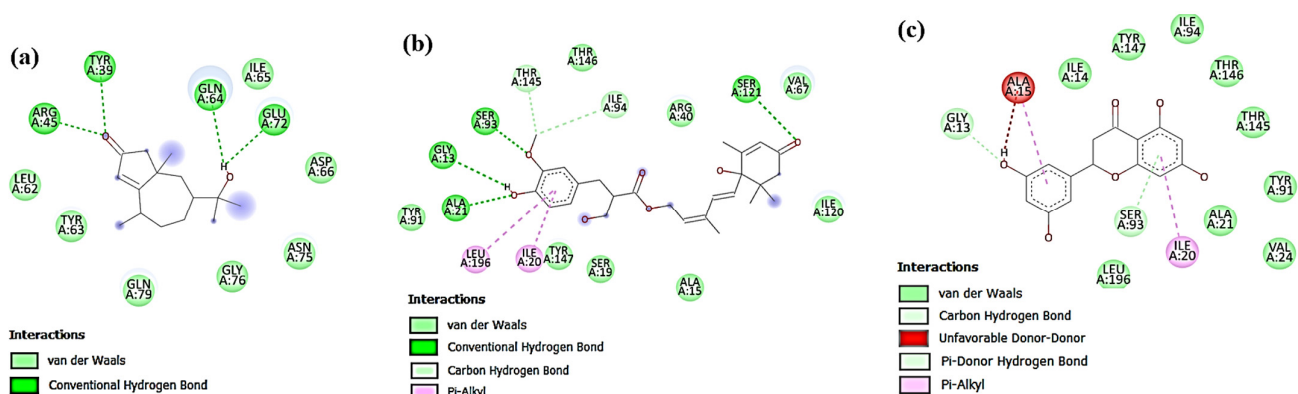


**Figure 5.** Two-dimensional (2D) molecular interactions of (a) Compound C3; (b) Compound C5; and (c) Compound C7 with enoyl-acyl carrier protein reductase of *S. aureus* (FabI) (PDB ID: 3GNS), (dimensions (Å); X:43.7680, Y: 51.7046, Z:49.0095), (root mean square deviation) RMSD < 2.

### 3.4.2. Docking against Cytotoxic Molecular Targets Interactions with $\beta$ -Catenin

In carcinogenesis, the Wnt/ $\beta$ -catenin signal pathway regulates cell proliferation, differentiation, and embryonic development [53].  $\beta$ -catenin is a signaling molecule in the Wnt pathway, which plays a central role in carcinogenicity [33,53]. Any impairment or activation of the Wnt pathway leads to cancerous diseases, such as breast, intestine, and prostate cancers [33]. The isolated compounds (**C1–C7**) were docked into the active site of  $\beta$ -catenin (PDB ID: 7AFW). They were found to bind to 205–210 and 243–251 amino acid residues with BFE between  $-4.2$  and  $-6.0$  kcal/mol (Table S6) [33]. The ligand **C5** showed a BFE of  $-5.1$  kcal/mol compared to the co-crystallized inhibitor R9Q ( $-6.2$  kcal/mol) and formed a distinct complement to the binding site while orienting the hydroxyl group toward the Thr205, and the benzene ring formed  $\pi$ -alkyl interactions with the backbone CH of Lys242 (Figure 6c). This moderate interaction was in full agreement with the obtained cytotoxic activity of **C5** (Table 3) and suggested the Wnt/ $\beta$ -catenin signal pathway as a potential mechanism for its cytotoxicity. Regarding compounds **C1** and **C2**, they showed low BFE values ( $-4.3$  and  $-4.2$  kcal/mol), although **C1** shared the co-crystallized inhibitor in binding with Asn206. Both compounds (**C1** and **C2**) interacted hydrophobically with Lys242 and Pro247 residues through  $\pi$ -alkyl interactions (Figure 6a,b) [33]. However, these results contradicted the obtained high cytotoxic activities of **C1/C2**, which suggested that they may act through another mechanism.

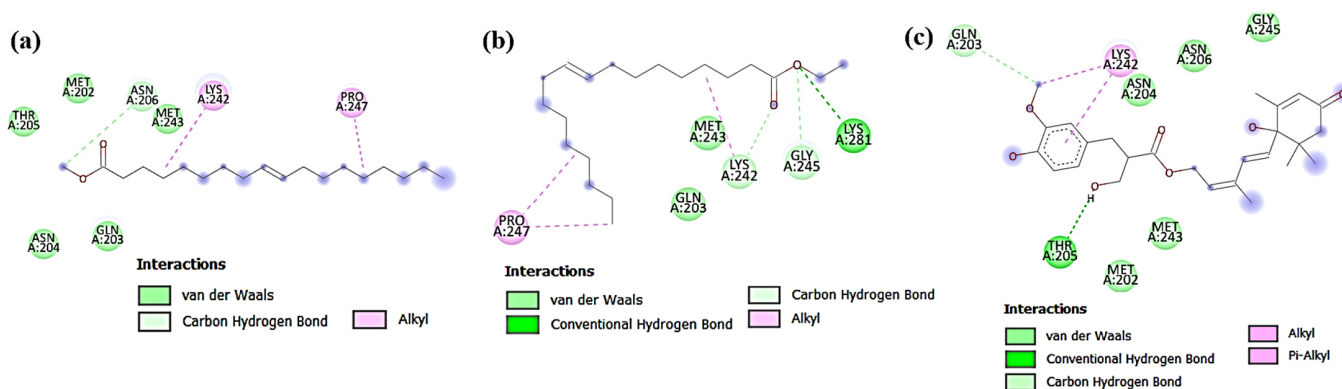


**Figure 6.** Two-dimensional (2D) molecular interactions of (a) Compound **C1** and (b) **C2**, and (c) **C5** with  $\beta$ -catenin (PDB ID:7AFW), (dimensions (Å); X:20.4162, Y: 21.1198, Z:25.0), (root mean square deviation) RMSD < 2.

### Interactions with Human Dihydrofolate Reductase (DHFR)

The human dihydrofolate reductase (DHFR) protein has a major role in DNA synthesis in the human and bacterial cell development process. Therefore, it could be considered a common target for both cytotoxicity and antimicrobial activities [34]. The tested compounds (**C1–C7**) displayed variable binding affinity to the DHFR protein with BFE values ranging from  $-3.8$  to  $-6.3$  kcal/mol in comparison with ciprofloxacin ( $-5.5$  kcal/mol) and methotrexate ( $-7.1$  kcal/mol) (Table S6). Compound **C5** showed good BFE ( $-5.3$  kcal/mol), which is comparable to ciprofloxacin, and showed H-bonding interactions with the amino acids Gly20, Ser118, Asp145, and Thr146 (Figure 7a), which is in full agreement with the result of the cytotoxic activity of this compound [33,34]. Notably, compound **C7** exhibited the highest BFE to DHFR enzyme ( $-6.3$  kcal/mol) among the other isolated compounds and shared ciprofloxacin in binding with Arg77, Ser118, and Ser119 residues (Figure 7b) [34]. Although compounds **C1** and **C2** showed low binding affinities, they exhibited binding to Ser119 and Lys55 residues and shared methotrexate in the interaction with Gly20 and Thr146 residues (Table S6) [34].

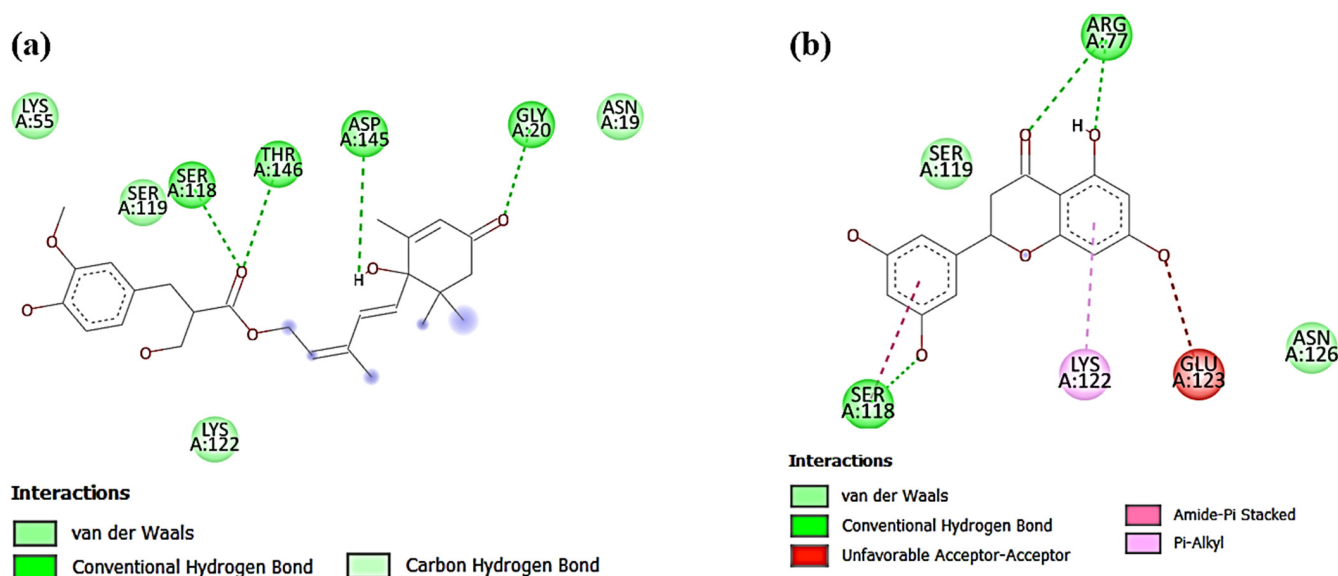


**Figure 7.** Two-dimensional (2D) molecular interactions of (a) compound C5; and (b) compound C7 with the crystal structure of human dihydrofolate reductase (DHFR) bound to NADPH (PDB ID:4M6J), (dimensions (Å); X:20.8191, Y:24.1576, Z:27.1117), (root mean square deviation) RMSD < 2.

#### Interactions with Human P-gp

The P-gp protein is a vital protein in MDR to anticancer drugs and other therapeutics by causing cellular efflux. Therefore, there is a necessity to discover safe MDR inhibitors [21]. Natural products represent a major source of safely used chemotherapeutic drugs [54]. The isolated compounds from *E. erinaceus* were virtually investigated for their binding to P-gp protein. In general, the *in silico* docking experiments predicted quite strong affinities of the investigated compounds toward P-gp, with BFE values ranging between  $-6.1$  and  $-8.4$  kcal/mol. Based on published data by Marques et al., 2021 [21], the preferred binding positions of the P-gp macromolecule are M or H sites. The inhibitors showed strong hydrophobic interactions at the M site of the macromolecule, the human P-gp (PDB ID: 6C0V), provided mainly by the multiple isoleucine, leucine, phenylalanine, serine, and tyrosine residues in the binding site (namely Ile340, 731, 735; Leu332, 339; Phe72, 314, 335, 336, 728, 732, 759, 983; Ser733, 979; and Tyr307, 310). Compound C3 (BFE,  $-7.7$  kcal/mol) exhibited hydrophobic interactions with Phe335, Leu339, Phe728, and Phe759 residues (Figure 8a). This was also observed in the case of C5 (BFE,  $-8.4$  kcal/mol), which showed several hydrophobic interactions with Phe335, Leu339, Phe759, Ile731, and Ile735 (Figure 8b). In some cases, such as in C1, C6, and C7, interactions with the hydroxyl or carbonyl groups of these ligands with Ser979, Ile736, and Ala729, respectively, were observed (Figures S42a,g and 8c). On the other hand, the hydroxyl or carbonyl groups present in other ligands, including C2, C3, C4, and C5, did not contribute much to any hydrophilic binding affinity (Table S6). Thus, the investigated compounds may act as potential MDR inhibitors via binding to P-gp protein.

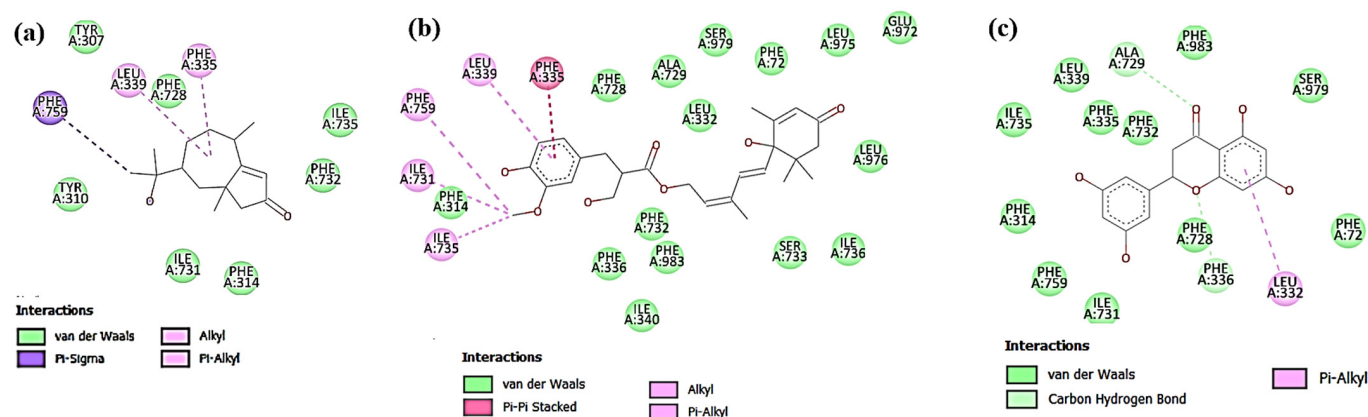


**Figure 8.** Two-dimensional (2D) molecular interactions of (a) Compound C3; (b) Compound C5; and (c) Compound C7 with the crystal structure of human P-gp (PDB ID: 6C0V), (dimensions (Å) X:20.8191, Y:24.1576, Z:27.1117), (root mean square deviation) RMSD < 2. Width 995, (root mean square deviation) RMSD < 2.

#### 4. Conclusions

The current study includes the chemical and biological evaluations of the Saudi wild plant *E. erinaceus*. Cytotoxic, antioxidant, and antimicrobial activities were investigated. The phytochemical investigation led to the isolation and identification of seven bioactive phytochemicals, including two unsaturated fatty acid esters, a pseudoguaiane sesquiterpene, a sesquiterpene lactone, two phenolics, and an abscisic alcohol derivative. Among the isolated compounds, two compounds were identified for the first time from nature viz., erinaceosin (a pseudoguaiane) and erinaceol (an abscisic alcohol derivative). In general, the results of this study demonstrated that the title plant has weak to moderate cytotoxic activity, however, it showed promising antibacterial, antifungal, and antioxidant properties. The results of the antimicrobial properties of the plant extracts and/or the fractions demonstrated that the total MeOH extract had the highest antimicrobial activity against all the tested strains except against *MRSA*. Compounds C1/C2 showed the highest cytotoxic activity against HCT-116 and CACO<sub>2</sub> cell lines. This research also demonstrated that the secondary metabolites isolated from *E. erinaceus* have variable degrees of binding affinity towards the active sites of selected target proteins, including DNA gyrase topoisomerase II, FabI,  $\beta$ -catenin, DHFR, and P-gp, which may contribute to their antimicrobial, anticancer, and multidrug-resistance inhibition mechanisms.

**Supplementary Materials:** The following supporting information can be downloaded at: <https://www.mdpi.com/article/10.3390/separations9120447/s1>, Figure S1–S37: Spectra of C1–C7; Tables S1–S4: NMR spectral data of C1, C2, C4, C6, and C7; Table S5: *In silico* physicochemical and pharmacokinetics of C1–C7; Table S6: Docking results of C1–C7 against PDB ID:1KZN, 3GNS, 7AFW, 4M6J, and 6C0V; Flowchart S1: Fractionation and purification of the CHCl<sub>3</sub> extract of *E. erinaceus*; Figure S38–S42: 2D molecular docking interactions of C1–C7 against PDB ID:1KZN, 3GNS, 7AFW, 4M6J, and 6C0V; Figure S43: Bioavailability radar representation of C1–C7; and Figure S44: Predicted BOILED-Egg diagram of C1–C7. Refs. [55,56] is cited in Supplementary Materials.

**Author Contributions:** Conceptualization, E.A.-S., M.M.E.-S. and O.D.E.-G.; methodology, S.H.S., F.M.A.B., A.I.F., M.H.A. and N.A.E.; compounds analysis and validation, S.H.S., F.M.A.B. and E.A.-S.; molecular docking software, S.H.S.; *in vitro* biological investigations, A.I.F., M.H.A. and N.A.E.; resources, A.I.F. and M.H.A.; writing-original draft, S.H.S., F.M.A.B. and E.A.-S.; review & editing, all authors; supervision, M.M.E.-S., O.D.E.-G. and E.A.-S. All authors have read and agreed to the published version of the manuscript.

**Funding:** This research received no external funding.

**Data Availability Statement:** The following supporting information can be downloaded at: [www.mdpi.com/xxx/s1](http://www.mdpi.com/xxx/s1), Figures S1–S37: Spectra of C1–C7; Tables S1–S4: NMR spectral data of C1, C2, C4, C6, and C7; Table S5: *In silico* physicochemical and pharmacokinetics of C1–C7; Table S6: Docking results of C1–C7 against PDB ID:1KZN, 3GNS, 7AFW, 4M6J, and 6C0V; Flowchart S1: Fractionation and purification of the CHCl<sub>3</sub> extract of *E. erinaceus*; Figures S38–S42: 2D molecular docking interactions of C1–C7 against PDB ID:1KZN, 3GNS, 7AFW, 4M6J, and 6C0V; Figure S43: Bioavailability radar representation of C1–C7; and Figure S44: Predicted BOILED-Egg diagram of C1–C7.

**Acknowledgments:** The authors would like to express a special thanks of gratitude to members of the Department of Pharmacognosy, Faculty of Pharmacy, Prince Sattam Bin Abdulaziz University, for their kind help and the use of lab facilities.

**Conflicts of Interest:** The authors declare no conflict of interest.

## References

1. Senejoux, F.; Demougeot, C.; Karimov, U.; Muyard, F.; Kerram, P.; Aisa, H.A.; Girard-Thernier, C. Chemical constituents from *Echinops integrifolius*. *Biochem. Syst. Ecol.* **2013**, *47*, 42–44. [[CrossRef](#)]
2. Dong, M.; Cong, B.; Yu, S.-H.; Sauriol, F.; Huo, C.-H.; Shi, Q.-W.; Gu, Y.-C.; Zamir, L.O.; Kiyota, H. Echinopines A and B: Sesquiterpenoids Possessing an Unprecedented Skeleton from *Echinops spinosus*. *Org. Lett.* **2008**, *10*, 701–704. [[CrossRef](#)] [[PubMed](#)]
3. Khadim, E.J.; Abdurassool, A.A.; Awad, Z.J. Phytochemical Investigation of Alkaloids in the Iraqi *Echinops heterophyllus* (Compositae). *Iraqi J. Pharm. Sci.* **2014**, *23*, 26–34. [[CrossRef](#)]
4. Kiyekbayeva, L.; Mohamed, N.M.; Yerkebulan, O.; Mohamed, E.I.; Ubaidilla, D.; Nursulu, A.; Assem, M.; Srivedavyasari, R.; Ross, S.A. Phytochemical constituents and antioxidant activity of *Echinops albicaulis*. *Nat. Prod. Res.* **2018**, *32*, 1203–1207. [[CrossRef](#)] [[PubMed](#)]
5. Lan, H.; Qi-Rong, C.; Rong, L.; Guo-Qiang, L.; Hao, H. A new pentacyclic triterpene, gmeliniin A, from *Echinops gmelinii* Turcz. *Chin. J. Chem.* **2000**, *18*, 112–114. [[CrossRef](#)]
6. Rolnik, A.; Olas, B. The Plants of the Asteraceae Family as Agents in the Protection of Human Health. *Int. J. Mol. Sci.* **2021**, *22*, 3009. [[CrossRef](#)]
7. Bulut, G.; Haznedaroglu, M.Z.; Dogan, A.; Koyu, H.; Tuzlaci, E. An ethnobotanical study of medicinal plants in Acipayam (Denizli-Turkey). *J. Herb. Med.* **2017**, *10*, 64–81. [[CrossRef](#)]
8. Menut, C.; Lamaty, G.; Weyerstahl, P.; Marschall, H.; Seelmann, I.; Amvam Zollo, P.H. Aromatic plants of tropical Central Africa. Part XXXI. Tricyclic sesquiterpenes from the root essential oil of *Echinops giganteus* var. *lelyi* C. D. Adams. *Flavour Fragr. J.* **1997**, *12*, 415–421. [[CrossRef](#)]
9. Bitew, H.; Hymete, A. The Genus *Echinops*: Phytochemistry and Biological Activities: A Review. *Front. Pharmacol.* **2019**, *10*, 1234. [[CrossRef](#)]
10. Mustafa, B.; Hajdari, A.; Krasniqi, F.; Hoxha, E.; Ademi, H.; Quave, C.L.; Pieroni, A. Medical ethnobotany of the Albanian Alps in Kosovo. *J. Ethnobiol. Ethnomed.* **2012**, *8*, 6. [[CrossRef](#)]
11. Abdallah, H.M.; Ezzat, S.M.; El Dine, R.S.; Abdel-Sattar, E.; Abdel-Naim, A.B. Protective effect of *Echinops galalensis* against CCl<sub>4</sub>-induced injury on the human hepatoma cell line (Huh7). *Phytochem. Lett.* **2013**, *6*, 73–78. [[CrossRef](#)]
12. Sharma, K.S.; Mishra, S.; Mehta, B.K. Antifertility activity of *Echinops echinatus* in albino rats. *Indian J. Med. Sci.* **1988**, *42*, 23–26.
13. Jin, Q.; Lee, J.W.; Jang, H.; Choi, J.E.; Kim, H.S.; Lee, D.; Hong, J.T.; Lee, M.K.; Hwang, B.Y. Dimeric sesquiterpene and thiophenes from the roots of *Echinops latifolius*. *Bioorg. Med. Chem. Lett.* **2016**, *26*, 5995–5998. [[CrossRef](#)]
14. Alam, M.K.; Ahmed, S.; Anjum, S.; Akram, M.; Shah, S.M.; Wariss, H.M.; Usmanghani, K. Evaluation of antipyretic activity of some medicinal plants from Cholistan desert Pakistan. *Pak. J. Pharm. Sci.* **2016**, *29*, 529–533.
15. Nakano, H.; Ali, A.; Ur Rehman, J.; Mamonov, L.K.; Cantrell, C.L.; Khan, I.A. Toxicity of thiophenes from *Echinops transiliensis* (Asteraceae) against *Aedes aegypti* (Diptera: Culicidae) larvae. *Chem. Biodivers.* **2014**, *11*, 1001–1009. [[CrossRef](#)]
16. Radulović, N.S.; Denić, M.S. Essential oils from the roots of *Echinops bannaticus* Rochel ex Schrad. and *Echinops sphaerocephalus* L. (Asteraceae): Chemotaxonomic and biosynthetic aspects. *Chem. Biodivers.* **2013**, *10*, 658–676. [[CrossRef](#)]
17. Sweilam, S.H.; Abdel Bar, F.M.; ElGindi, O.D.; El-Sherei, M.M.; Abdel-Sattar, E.A. Chemical and In Vitro Anti-inflammatory Assessment of *Echinops erinaceus*. *Trop. J. Nat. Prod. Res.* **2021**, *5*, 715–719.
18. Gillet, J.-P.; Gottesman, M.M. Mechanisms of multidrug resistance in cancer. In *Multi-Drug Resistance in Cancer*; Springer: Berlin/Heidelberg, Germany, 2010; pp. 47–76.
19. Wróbel, A.; Eklund, P.; Bobrowska-Hägerstrand, M.; Hägerstrand, H. Lignans and norlignans inhibit multidrug resistance protein 1 (MRP1/ABCC1)-mediated transport. *Anticancer Res.* **2010**, *30*, 4423–4428.
20. Luo, L.; Yang, J.; Wang, C.; Wu, J.; Li, Y.; Zhang, X.; Li, H.; Zhang, H.; Zhou, Y.; Lu, A.; et al. Natural products for infectious microbes and diseases: An overview of sources, compounds, and chemical diversities. *Sci. China Life Sci.* **2022**, *65*, 1123–1145. [[CrossRef](#)]



21. Marques, S.M.; Šupolíková, L.; Molčanová, L.; Šmejkal, K.; Bednar, D.; Slaninová, I. Screening of Natural Compounds as P-Glycoprotein Inhibitors against Multidrug Resistance. *Biomedicines* **2021**, *9*, 357. [[CrossRef](#)]
22. Bhabha, G.; Ekiert, D.C.; Jennewein, M.; Zmasek, C.M.; Tuttle, L.M.; Kroon, G.; Dyson, H.J.; Godzik, A.; Wilson, I.A.; Wright, P.E. Divergent evolution of protein conformational dynamics in dihydrofolate reductase. *Nat. Struct. Mol. Biol* **2013**, *20*, 1243–1249. [[CrossRef](#)] [[PubMed](#)]
23. Mosmann, T. Rapid colorimetric assay for cellular growth and survival: Application to proliferation and cytotoxicity assays. *J. Immunol. Methods* **1983**, *65*, 55–63. [[CrossRef](#)] [[PubMed](#)]
24. Abd-El-Aziz, A.S.; El-Ghezlani, E.G.; Elaasser, M.M.; Afifi, T.H.; Okasha, R.M. First example of cationic cyclopentadienyliron based chromene complexes and polymers: Synthesis, characterization, and biological applications. *J. Inorg. Organomet. Polym. Mater.* **2020**, *30*, 131–146. [[CrossRef](#)]
25. Gomha, S.M.; Riyadh, S.M.; Mahmmoud, E.A.; Elaasser, M.M. Synthesis and Anticancer Activities of Thiazoles, 1,3-Thiazines, and Thiazolidine Using Chitosan-Grafted-Poly(vinylpyridine) as Basic Catalyst. *Heterocycles* **2015**, *91*, 1227–1243.
26. Mishra, V.; Prasad, D.N. Application of in vitro methods for selection of Lactobacillus casei strains as potential probiotics. *Int. J. Food Microbiol.* **2005**, *103*, 109–115. [[CrossRef](#)]
27. Burits, M.; Bucar, F. Antioxidant activity of *Nigella sativa* essential oil. *Phytother. Res.* **2000**, *14*, 323–328. [[CrossRef](#)]
28. Foudah, A.I.; Alqarni, M.H.; Alam, A.; Salkini, M.A.; Ross, S.A.; Yusufoglu, H.S. Phytochemical Screening, In Vitro and In Silico Studies of Volatile Compounds from *Petroselinum crispum* (Mill) Leaves Grown in Saudi Arabia. *Molecules* **2022**, *27*, 934. [[CrossRef](#)]
29. Filimonov, D.A.; Lagunin, A.A.; Glorizova, T.A.; Rudik, A.V.; Druzhilovskii, D.S.; Pogodin, P.V.; Poroikov, V.V. Prediction of the Biological Activity Spectra of Organic Compounds Using the Pass Online Web Resource. *Chem. Heterocycl. Compd.* **2014**, *50*, 444–457. [[CrossRef](#)]
30. Daina, A.; Michielin, O.; Zoete, V. SwissADME: A free web tool to evaluate pharmacokinetics, drug-likeness and medicinal chemistry friendliness of small molecules. *Sci. Rep.* **2017**, *7*, 42717. [[CrossRef](#)]
31. Lafitte, D.; Lamour, V.; Tsvetkov, P.O.; Makarov, A.A.; Klich, M.; Deprez, P.; Moras, D.; Briand, C.; Gilli, R. DNA gyrase interaction with coumarin-based inhibitors: The role of the hydroxybenzoate isopentenyl moiety and the 5'-methyl group of the noviose. *Biochemistry* **2002**, *41*, 7217–7223. [[CrossRef](#)]
32. Priyadarshi, A.; Kim, E.E.; Hwang, K.Y. Structural insights into *Staphylococcus aureus* enoyl-ACP reductase (FabI), in complex with NADP and triclosan. *Proteins* **2010**, *78*, 480–486. [[CrossRef](#)]
33. Kessler, D.; Mayer, M.; Zahn, S.K.; Zeeb, M.; Wöhrle, S.; Bergner, A.; Bruchhaus, J.; Ciftci, T.; Dahmann, G.; Dettling, M.; et al. Getting a Grip on the Undrugged: Targeting  $\beta$ -Catenin with Fragment-Based Methods. *ChemMedChem* **2021**, *16*, 1420–1424. [[CrossRef](#)]
34. Khatun, M.; Muhit, M.; Hossain, M.J.; Al-Mansur, M.; Rahman, S.M. Isolation of phytochemical constituents from *Stevia rebaudiana* (Bert.) and evaluation of their anticancer, antimicrobial and antioxidant properties via in vitro and in silico approaches. *Heliyon* **2021**, *7*, e08475. [[CrossRef](#)]
35. Chira, N.; Nicolescu, A.; Raluca, S.; Rosca, S. Fatty Acid Composition of Vegetable Oils Determined from  $^{13}\text{C}$ -NMR Spectra. *Rev. Chim. (Bucharest)* **2016**, *67*, 1257–1263.
36. Di Pietro, M.E.; Mannu, A.; Mele, A. NMR Determination of Free Fatty Acids in Vegetable Oils. *Processes* **2020**, *8*, 410. [[CrossRef](#)]
37. Hymete, A.; Rohloff, J.; Kjøsen, H.; Iversen, T.-H. Acetylenic thiophenes from the roots of *Echinops ellenbeckii* from Ethiopia. *Nat. Prod. Res.* **2005**, *19*, 755–761. [[CrossRef](#)]
38. Lao, A.; Fujimoto, Y.; Tatsuno, T. Studies on the Constituents of *Artemisia argyi* LEVL et VANT. *Chem. Pharm. Bull.* **1984**, *32*, 723–727. [[CrossRef](#)]
39. Atta-Ur-Rahman; Ahmad, V.U.  $^{13}\text{C}$ -NMR of Natural Products: Volume 1 Monoterpenes and Sesquiterpenes, 1st ed.; Springer: Boston, MA, USA, 1992; Volume 1, pp. X–966.
40. Yuan, Z.; Zheng, X.; Zhao, Y.; Liu, Y.; Zhou, S.; Wei, C.; Hu, Y.; Shao, H. Phytotoxic Compounds Isolated from Leaves of the Invasive Weed *Xanthium spinosum*. *Molecules* **2018**, *23*, 2840. [[CrossRef](#)]
41. Silva, J.; Alves, C.; Martins, A.; Susano, P.; Simões, M.; Guedes, M.; Rehfeldt, S.; Pinteus, S.; Gaspar, H.; Rodrigues, A.; et al. Loliolide, a New Therapeutic Option for Neurological Diseases? In Vitro Neuroprotective and Anti-Inflammatory Activities of a Monoterpenoid Lactone Isolated from *Codium tomentosum*. *Int. J. Mol. Sci.* **2021**, *22*, 1888. [[CrossRef](#)]
42. Milborrow, B.V. The conformation of abscisic acid by NMR. and a revision of the proposed mechanism for cyclization during its biosynthesis. *Biochem. J.* **1984**, *220*, 325–332. [[CrossRef](#)] [[PubMed](#)]
43. Ferreres, F.; Andrade, P.; Tomás-Barberán, F.A. Natural Occurrence of Abscisic Acid in Heather Honey and Floral Nectar. *J. Agric. Food Chem.* **1996**, *44*, 2053–2056. [[CrossRef](#)]
44. Frackenpohl, J.; Grill, E.; Bojack, G.; Baltz, R.; Busch, M.; Dittgen, J.; Franke, J.; Freigang, J.; Gonzalez, S.; Heinemann, I.; et al. Insights into the *in Vitro* and *in Vivo* SAR of Abscisic Acid—Exploring Unprecedented Variations of the Side Chain via Cross-Coupling-Mediated Syntheses. *Eur. J. Org. Chem.* **2018**, *2018*, 1403–1415. [[CrossRef](#)]
45. Jo, M.S.; Lee, S.; Yu, J.S.; Baek, S.C.; Cho, Y.-C.; Kim, K.H. Megastigmmane Derivatives from the Cladodes of *Opuntia humifusa* and Their Nitric Oxide Inhibitory Activities in Macrophages. *J. Nat. Prod.* **2020**, *83*, 684–692. [[CrossRef](#)] [[PubMed](#)]
46. Ng, V.A.; Ago, E.M.; Shen, C.-C.; Ragasa, C. Chemical Constituents of *Cycas aenigma*. *J. Appl. Pharm. Sci* **2015**, *5*, 32–36. [[CrossRef](#)]
47. Sytar, O.; Hemmerich, I.; Zivcak, M.; Rauh, C.; Brestic, M. Comparative analysis of bioactive phenolic compounds composition from 26 medicinal plants. *Saudi J. Biol. Sci.* **2016**, *25*, 631–641. [[CrossRef](#)]

48. Nessa, F.; Ismail, Z.; Mohamed, N. Xanthine oxidase inhibitory activities of extracts and flavonoids of the leaves of *Blumea balsamifera*. *Pharm. Biol.* **2010**, *48*, 1405–1412. [[CrossRef](#)]
49. Ayyad, S.E.; Abdel-Lateff, A.; Alarif, W.M.; Patacchioli, F.R.; Badria, F.A.; Ezmirly, S.T. In vitro and in vivo study of cucurbitacins-type triterpene glucoside from *Citrullus colocynthis* growing in Saudi Arabia against hepatocellular carcinoma. *Environ. Toxicol. Pharmacol.* **2012**, *33*, 245–251. [[CrossRef](#)]
50. Daina, A.; Zoete, V. A BOILED-Egg To Predict Gastrointestinal Absorption and Brain Penetration of Small Molecules. *ChemMed-Chem* **2016**, *11*, 1117–1121. [[CrossRef](#)]
51. Bojarska, J.; Remko, M.; Breza, M.; Madura, I.D.; Kaczmarek, K.; Zabrocki, J.; Wolf, W.M. A Supramolecular Approach to Structure-Based Design with A Focus on Synthons Hierarchy in Ornithine-Derived Ligands: Review, Synthesis, Experimental and in Silico Studies. *Molecules* **2020**, *25*, 1135. [[CrossRef](#)]
52. Kandsi, F.; Elbouzidi, A.; Lafdil, F.Z.; Meskali, N.; Azghar, A.; Addi, M.; Hano, C.; Maleb, A.; Gseyra, N. Antibacterial and Antioxidant Activity of *Dysphania ambrosioides* (L.) Mosyakin and Clemants Essential Oils: Experimental and Computational Approaches. *Antibiotics* **2022**, *11*, 482. [[CrossRef](#)]
53. He, S.; Tang, S. WNT/ $\beta$ -catenin signaling in the development of liver cancers. *Biomed. Pharmacother.* **2020**, *132*, 110851. [[CrossRef](#)]
54. Li, W.; Zhang, H.; Assaraf, Y.G.; Zhao, K.; Xu, X.; Xie, J.; Yang, D.H.; Chen, Z.S. Overcoming ABC transporter-mediated multidrug resistance: Molecular mechanisms and novel therapeutic drug strategies. *Drug Resist. Updates* **2016**, *27*, 14–29. [[CrossRef](#)]
55. Guzel, A.; Aksit, H.; Elmastas, M.; Erenler, R. Bioassay-guided isolation and identification of antioxidant flavonoids from *Cyclotrichium origanifolium* (Labill.) Manden and Scheng. *Pharmacogn. Mag.* **2017**, *13*, 316–320. [[CrossRef](#)]
56. Hussein, N.; Amen, Y.; Abdel Bar, F.; Halim, A.; Saad, H.-E. Antioxidants and  $\alpha$ -Glucosidase Inhibitors from *Lactuca serriola* L. *Rec. Nat. Prod.* **2020**, *14*, 410–415. [[CrossRef](#)]